Journal of Assisted Reproduction and Genetics (2020) 37:1431–1439
https://doi.org/10.1007/s10815-020-01770-1

GENETICS

A novel homozygous mutation in *WDR19* induces disorganization of microtubules in sperm flagella and nonsyndromic asthenoteratospermia

Xiaoqing Ni[1,2,3] · Jiajia Wang[1,2,3] · Mingrong Lv[1,4,5] · Chunyu Liu[6,7,8] · Yading Zhong[9] · Shixiong Tian[6,7,8] · Huan Wu[1,2,3] · Huiru Cheng[1,2,3] · Yang Gao[1,2,3] · Qing Tan[1,2,3] · Beili Chen[1,2,3] · Qiang Li[4,5] · Bing Song[1,4,5] · Zhaolian Wei[1,2,3] · Ping Zhou[1,2,3] · Xiaojin He[1,2,3] · Feng Zhang[6,7,8] · Yunxia Cao[1,2,3]

Received: 25 December 2019 / Accepted: 31 March 2020 / Published online: 23 April 2020

Abstract

Background Asthenoteratospermia with multiple morphological abnormalities in the sperm flagella (MMAF) is a significant cause of male infertility. WDR19 is a core component in the IFT-A complex and has a critical role in intraflagellar transport. However, the role of *WDR19* mutations in male infertility has yet to be examined.

Methods and results We performed whole exome sequencing (WES) for 65 asthenoteratospermia individuals and identified a proband who carried a homozygous *WDR19* (c.A3811G, p.K1271E) mutation from a consanguineous family. Systematic examinations, including CT scanning and retinal imaging, excluded previous ciliopathic syndromes in the proband. Moreover, semen analysis of this patient showed that the progressive rate decreased to zero, and the sperm flagella showed multiple morphological abnormalities. Scanning and transmission electron microscopy assays indicated that the ultrastructure of sperm flagella in the patient was completely destroyed, while immunofluorescence revealed that WDR19 was absent from the sperm neck and flagella. Moreover, IFT140 and IFT88, predicted to interact with WDR19 directly, were mis-allocated in the *WDR19*-mutated sperm. Notably, the MMAF subject harboring *WDR19* variant and his partner successfully achieved clinical pregnancy through intracytoplasmic sperm injection (ICSI).

Conclusions We identified *WDR19* as a novel pathogenic gene for male infertility caused by asthenoteratospermia in the absence of other ciliopathic phenotypes, and that patients carrying *WDR19* variant can have favorable pregnancy outcomes following ICSI.

Keywords Asthenoteratospermia · WDR19 · Flagellum · Whole exome sequencing · Intracytoplasmic sperm injection

Xiaoqing Ni and Jiajia Wang contributed equally to this work.

Electronic supplementary material The online version of this article (https://doi.org/10.1007/s10815-020-01770-1) contains supplementary material, which is available to authorized users.

✉ Xiaojin He
hxj0117@126.com

✉ Feng Zhang
feng.fudan@gmail.com

✉ Yunxia Cao
caoyunxia6@126.com

[1] Reproductive Medicine Center, Department of Obstetrics and Gynecology, The First Affiliated Hospital of Anhui Medical University, Hefei, China

[2] NHC Key Laboratory of Study on Abnormal Gametes and Reproductive Tract, Anhui Medical University, Hefei, China

[3] Key Laboratory of Population Health Across Life Cycle (Anhui Medical University), Ministry of Education of the People's Republic of China, Hefei, China

[4] Anhui Province Key Laboratory of Reproductive Health and Genetics, Anhui Medical University, Hefei 230022, China

[5] Anhui Provincial Engineering Technology Research Center for Biopreservation and Artificial Organs, Hefei 230022, China

[6] Obstetrics and Gynecology Hospital, NHC Key Laboratory of Reproduction Regulation (Shanghai Institute of Planned Parenthood Research), State Key Laboratory of Genetic Engineering at School of Life Sciences, Fudan University, Shanghai 200011, China

[7] Shanghai Key Laboratory of Female Reproductive Endocrine Related Diseases, Shanghai 200011, China

[8] State Key Laboratory of Reproductive Medicine, Center for Global Health, School of Public Health, Nanjing Medical University, Nanjing 211116, China

[9] Department of Pathology, The First Affiliated Hospital of Anhui Medical University, Hefei 230022, China

Introduction

Asthenoteratospermia is characterized by a marked decrease in sperm motility and multiple morphological abnormalities of the flagella (MMAF), and is one of primary causes of male infertility. Previous genetic studies on sperm flagellar deformity have shown that functional deficiencies in flagella-related genes are the main cause of asthenoteratospermia with MMAF in humans and mice [1].

Intraflagellar transport (IFT) is required for proper flagellar development and maintenance and, thus, plays an important role in spermatogenesis and male fertility [2, 3]. WD repeat-containing protein 19 (WDR19), also known as IFT144 (MIM 608151), is a core component in the intraflagellar transport complex A (IFT-A). The function of WDR19 in cilia was first described in *Caenorhabditis elegans* to be critical in maintaining structural and functional integrity in the IFT machinery [4]. A series of subsequent studies confirmed that mutations in *WDR19* are involved in various ciliopathies, including Sensenbrenner syndrome, Jeune syndrome, Caroli syndrome, nephronophthisis (NHPH), and autosomal recessive retinitis pigmentosa (arRP). However, to date, the relationship between WDR19 and male infertility has not been examined. Moreover, the impacts that *WDR19* mutations have on the ultrastructures of flagella and cilia, as well as their associated mechanisms, remain unknown.

In this study, we performed whole exome sequencing (WES) for 65 Han Chinese men affected by asthenoteratospermia, and identified a novel homozygous mutation in *WDR19* in one patient. Furthermore, systematic clinical examinations and functional studies were performed to investigate the impacts of different *WDR19* mutations and explore their pathogenesis. Intracytoplasmic sperm injection (ICSI) was used to aid in fertilization and pregnancy in the *WDR19*-mutated patient.

Materials and methods

Subjects and clinical investigation

A total of 65 patients diagnosed with severe asthenoteratospermia characterized by multiple flagella malformations, including absent, short, bent, coiled, and/or irregular sperm tails, were enrolled from the First Affiliated Hospital of Anhui Medical University in China. None of the patients had obvious primary ciliary dyskinesia-related symptoms, such as bronchitis, sinusitis, otitis media, or pneumonia. All individuals had normal somatic karyotypes (46, XY), with no Y chromosome microdeletions. Peripheral whole blood samples from the patients were collected for subsequent genetic analysis.

Semen characteristics and sperm morphological analysis

Fresh semen from the patients and normal male controls was collected and examined in accordance with the WHO guidelines (5th edition) [5]. Sperm morphology was analyzed using hematoxylin and eosin (H&E) staining.

This study was approved by the Ethics Committee of the First Affiliated Hospital of Anhui Medical University. Written consent was obtained from the patients and their family members, as well as the fertile control male subjects.

WES and bioinformatic analysis

Genomic DNA was extracted from whole peripheral blood for WES. Details on the methods used for analysis were described previously [6]. A pipeline illustration can be found in online supplementary figure 1.

Immunofluorescence assays

Sperm cells were preproccessed following previously published procedures [6] and incubated overnight at 4 °C with the following primary antibodies: rabbit polyclonal anti-WDR19 (13647-1-AP, proteintech, 1:100), anti-IFT140 (17460-1-AP, proteintech, 1:500), anti-IFT88 (13967-1-AP, proteintech, 1:100), anti-SPAG6 (bs-12291R, Bioss, 1:200), and anti-acetylated alpha-tubulin (5335S, CST, 1:500). Washes were performed using phosphate buffer saline (PBS), followed by 1-h incubation at 25 °C with highly cross-adsorbed secondary antibodies at a dilution of 1:500. The antibodies employed in this analysis were as follows: anti-rabbit-Alexa Fluor-594 anti-WDR19, anti-IFT140, anti-IFT88, and anti-mouse-Alexa Fluor-488 for anti-acetylated alpha-tubulin. Images were captured with a confocal microscope (Zeiss LSM 710).

Reverse transcription PCR and real-time quantitative PCR

Total RNA (1 μg) of sperm was extracted using the RNeasy Mini Kit (QIAGEN) and converted into cDNAs using SuperScript III Reverse Transcriptase (Invitrogen) and oligo (dT) primers (TaKaRa). The obtained cDNAs were used in subsequent real-time fluorescence quantitative PCR analysis with transcript-specific primers (online supplementary table 1). ACTIN was used as an internal control. The expression of mRNA was quantified according to the 2-DDCt method.

Scanning and transmission electron microscopy

For scanning electron microscopy (SEM) and transmission electron microscopy (TEM), spermatozoa were prepared in

accordance with the protocol described previously. [6] Specifically, for SEM, the samples were subsequently dehydrated in a series of ethanol dilutions at increasing concentrations and dried with hexamethyldisilazane (HMDS). Samples were then air-dried, added dropwise to the specimen stubs, sputter coated, and examined via field emission scanning electron microscopy (Nova nano 450, Thermo Fisher).

Clinical and laboratory examinations

CT scanning was used to examine the patient's bones, liver, and kidneys. Panoramic photography was used to examine the patient's teeth. Photographs of the retina were used to observe the fundus, macula, and fundus arterioles. Liver and kidney function testing was also performed.

Assisted reproductive procedures

The partner of the proband was treated with standard control ovarian stimulation by a long protocol of gonadotrophin administration. After oocyte collection, ICSI was conducted as previously described [7]. The fertilization rate was assessed 18–19 h after ICSI. The embryos were cultured in cleavage medium and then blastocyst medium (Cook Medical, USA) and incubated to day 5 or day 6. Two viable embryos were transferred into the female partner's uterus in a fresh cycle. Clinical pregnancy was confirmed by detection of a fetal heartbeat 5 weeks after embryo transfer.

Results

In this study, we identified a homozygous variant in 1 (1.5%) of 65 human cases in the novel asthenoteratospermia candidate gene *WDR19* (Fig. 1). The semen volume of the patient was 1.8 mL, and the sperm concentration was 61.6×10^6/mL. However, the progressive motility rate was determined to be zero. Sperm morphology was assessed by H&E staining and compared with those of fertile individuals [8]. A significant proportion of the proband's sperm presented with typical MMAF features, including coiled (52.0%), short (15.5%), angulation (12.0%), absent flagella (4.5%), and irregular calibre (2.5%). The remaining 13.5% of the sperm cells were found to have normal flagella (Fig. 2A–D and Table 1).

Due to the consanguineous status of the family, we postulated that the causative mutation may be a rare homozygous mutation within the general human population (Fig. 1). Loss-of-function variants and potentially deleterious missense variants predicted by Sorting Intolerant From Tolerant (SIFT), PolyPhen-2, and MutationTaster were given preference (online supplementary table 2 and online supplementary figure 1). In addition, the genes expressed in testis were preferentially examined. Interestingly, the proband carried a rare homozygous *WDR19* c.A3811G (p.K1271E) missense mutation, which was verified by Sanger sequencing. Both parents were determined to be heterozygous carriers (Fig. 1A). However, this *WDR19* missense mutation was absent from the human population genome data including 1000 Genomes Project, Esp6500s, and Genome Aggregation Database (online supplementary table 2). Further, the PolyPhen-2 and MutationTaster tools suggest that the *WDR19* c.A3811G mutation is damaging. These findings indicate that the identified homozygous missense mutation in *WDR19* could be pathogenic.

Immunofluorescence staining revealed that within healthy control sperm, WDR19 is highly expressed in the sperm neck and flagella in a punctate pattern along the axoneme. However, WDR19 was absent from the sperm of the *WDR19*-mutated patient (Fig. 2O–V). Moreover, q-PCR showed that the mRNA level of *WDR19* in sperm was significantly decreased in the *WDR19*-mutated patient when compared with that of the health control (online supplementary figure 2). Additionally, IFT140 immunostaining appeared to be localized in the middle of sperm head and the flagellum in the control subject, but it was abnormally accumulated in the top of sperm head and sperm neck from *WDR19*-mutated men. Similarly, IFT88 immunostaining appeared to be localized in the sperm manchette and the flagellum in the control subject; however, it was abnormally located in the sperm neck from *WDR19*-mutated men. SPAG6 is a component of the central apparatus of the 9 + 2 axoneme. SPAG6 immunostaining normally localized along the sperm flagella in the control normal sperm. However, it was absent in the sperm from *WDR19*-mutated subjects (online supplementary Fig. 3).

Under SEM, WDR19-deficient sperm primarily appeared with short and coiled flagella (Fig. 2K). TEM analysis was performed on 100 random cross sections of sperm flagella. The proportion of the following structures in the *WDR19*-mutated patient and the normal control was assessed: (i) the typical 9+2 microtubule arrangement (nine fused peripheral microtubule pairs with two unfused microtubules at the center), (ii) 9+0 or 9+1 microtubule arrangement (disappearance or partial disappearance of central microtubules), and (iii) complete absence of microtubules. Significant structural differences were noted between the *WDR19*-mutated patient and healthy control man ($P < 0.0001$) (Fig. 2E, 2F). The typical "9+2" arrangement in normal spermatozoa was observed in the control man (Fig. 2H–J). However, in the *WDR19*-mutated patient, a distinct appearance predominated consisting of a mostly vacuolar cross-sectional phenotype, damaged axoneme, and absence of microtubule structures, with only small amounts of debris-like substances. The remaining sperm contained 9 peripheral microtubule (PM) doublets, yet lacked the central pair (CP) of microtubules (9+0

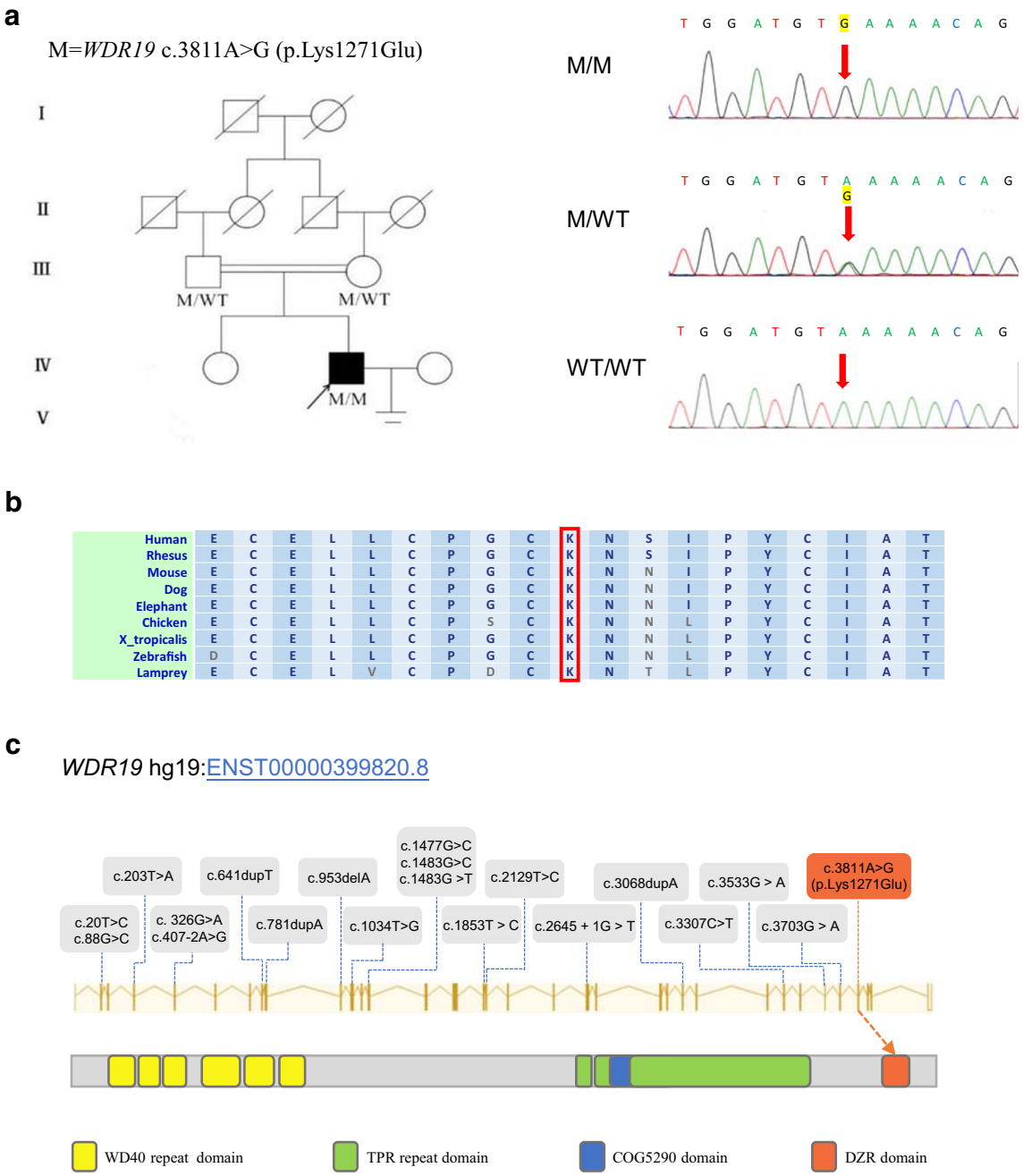

Fig. 1 Mutations of *WDR19* in the patient and previous studies. (A) The pedigree of the investigated family affected by the variant *WDR19* c.3811A>G. Sanger sequencing results are shown on the right side of the pedigree. I through V represent a total of five generations from the oldest to the youngest. Samples from generations I and II of the family were not available for genetic analysis. The mutated position is indicated by red arrows. (B) The mutated position of WDR19 is conserved among species. (C) Mutations of *WDR19* identified in previous studies (gray box) and this study (red box). The WDR19 protein contains six WD40 repeat domains, three tetratricopeptide (TPR) repeat domains, a COG5290 domain, and a DZR domain. The *WDR19* c.A3811G mutation is specifically occurred in the DZR domain. M, *WDR19* mutation; WT, wild type

arrangement; Fig. 2L–N). All analyzed cross sections of sperm flagella from the *WDR19*-mutated patient were abnormal.

To determine whether the patient exhibited other systemic symptoms, we carried out a general examination. CT imaging revealed no obvious abnormalities within the long bones, phalanxes, ribs, and pelvis. There were also no obvious abnormalities in the liver, and no intrahepatic bile duct dilatation was observed. No cysts or fibrosis in the liver or kidney was observed. Photographs of the retina showed normal fundus, macula, and fundus arterioles. Panoramic photography showed no obvious deformity of the patient's teeth (online supplementary figure 4). Lastly, laboratory blood analysis showed normal liver and kidney function.

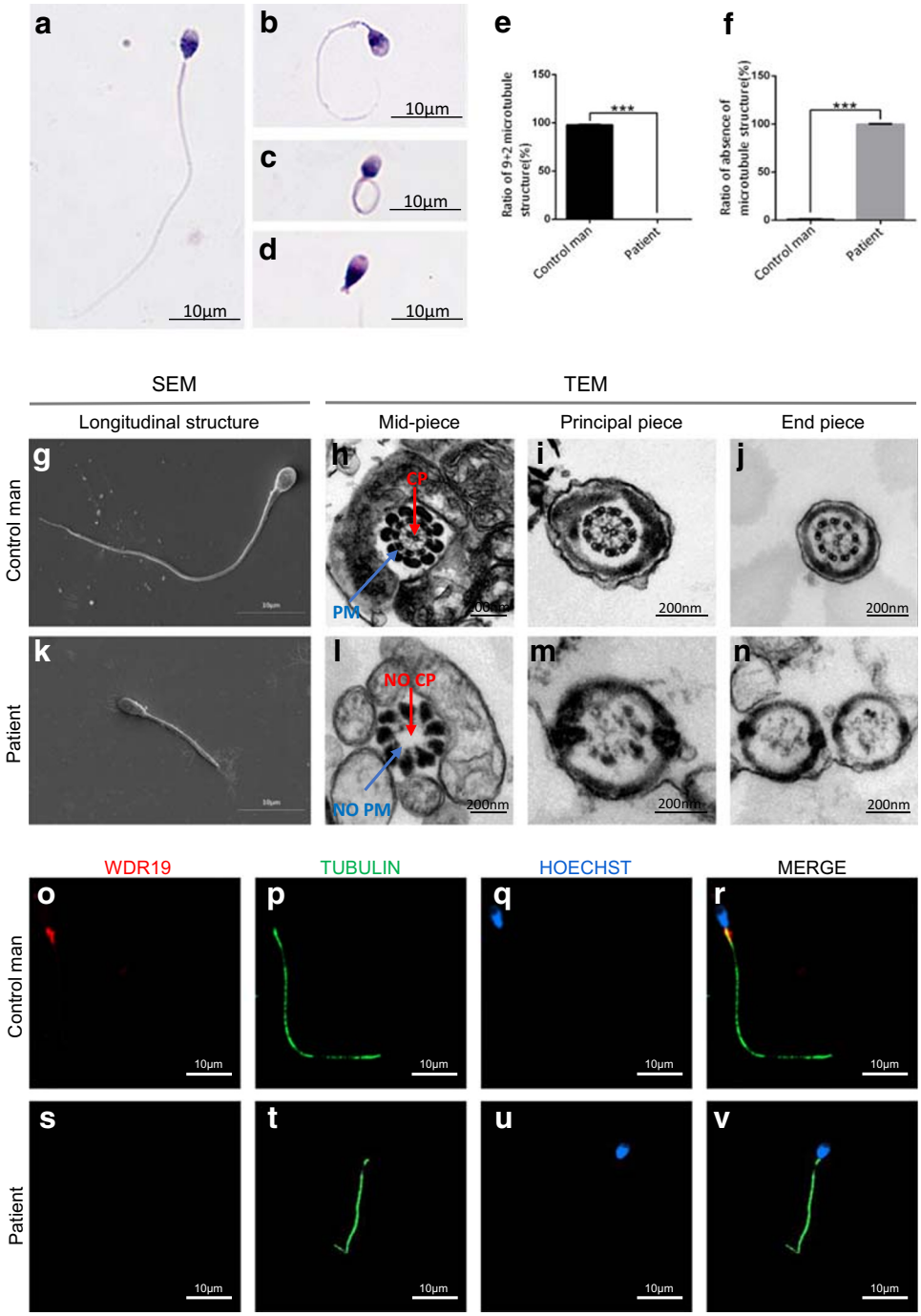

Fig. 2 Sperm morphologies and immunofluorescence assays in the *WDR19*-mutated patient. (A) Normal morphology of a spermatozoon from a healthy control man. Most spermatozoa of the patient presented with multiple morphological abnormalities, including short (B), coiled (C), absent flagella (D). (E–N) SEM and TEM analyses were conducted in the spermatozoa from a control man and the *WDR19*-mutated patient. There were significant differences in the number of "9+2" microtubule structure ($P < 0.0001$; E) and the number of absence of microtubule structure ($P < 0.0001$; F) in spermatozoa between the patient and a healthy control. SEM showed long flagella in the control man (G), and short flagella in the patient (K). TEM showed the typical "9+2" microtubule structure of a normal spermatozoa (H–J) and a completely destroyed microtubule structure in the patient (L–N). (O–V) WDR19 immunostaining (red) was primarily concentrated at the sperm neck and flagellum, and appeared in a punctate pattern along the axoneme in the control man (O–R), while the WDR19 immunostaining was absent in the sperm of the *WDR19*-mutated patient (S–V). DNA (blue) was counterstained with Hoechst as a nuclear marker. The anti-acetylated alpha-tubulin (green) staining uniformly displays the full-length flagellum in the control, whereas the sperm flagellar morphologies are abnormal in the *WDR19*-mutated patient. Scale bars: 10 μm. CP, central pair of microtubules; PM, peripheral microtubule doublets; SEM, scanning electron microscopy; TEM, transmission electron microscopy

Table 1 Semen characteristics and sperm morphologies in the *WDR19*-mutated patient

	Patient	Reference limits*
Semen parameter		
Semen volume (mL)	1.8	> 1.5
Sperm concentration (10^6/mL)	61.6	> 15.0
Motility (%)	0.0	> 40.0
Progressive motility (%)	0.0	> 32.0
Sperm morphology		
Absent flagella (%)	4.5	< 5.0
Short flagella (%)	15.5	< 1.0
Coiled flagella (%)	52.0	< 17.0
Angulation (%)	12.0	< 13.0
Irregular calibre (%)	2.5	< 2.0
Normal flagella (%)	13.5	> 23.0

*Reference limits according to the WHO standards and the distribution range of morphologically normal spermatozoa observed in 926 fertile individuals [5, 8]

Since the sperm motility rate was determined to be zero, ICSI was performed in the proband and his wife. Eleven oocytes were retrieved at metaphase II and 8 were fertilized by ICSI with the patient's own sperm. Gardner blastocyst grading system was used to evaluate blastocyst quality. Embryos with grades exceeding 3BB were considered high quality. In this case, two good quality blastocysts (5BB, 3BB) (Fig. 3) were obtained and used in a frozen embryo transfer. The couple achieved a single successful clinical pregnancy. The results suggest that patient harboring *WDR19* mutation has a good prognosis using ICSI.

Discussion

WDR19 encodes a large protein, IFT144, composed of 1342 amino acids. Data from the NCBI database showed that the protein contained six WD40 repeats, three TPR repeats, one COG5290, and one double zinc ribbon (DZR) domain (https://www.ncbi.nlm.nih.gov/protein/). Sequence analysis has revealed that the *WDR19* gene is conserved from *Caenorhabditis elegans* to humans. In *Caenorhabditis elegans* and mice, mutated forms of IFT144 cause a slight reduction in the number of cilia and simultaneously cause shortening of the cilia and accumulation of many IFT particles along the axons [4]. Additionally, deficiency of DYF-2 (orthologue of human WDR19) selectively affects the assembly and motility of IFT components, and leads to defects in axoneme structure and chemosensation in nematodes [4]. In previous studies, defects in various IFT-A and IFT-B components were shown to cause damage to the development of flagella in humans and mice, and lead to asthenospermia-induced infertility [9, 10].

Further, previous studies identified human individuals carrying *WDR19* mutations, including missense, insertions, deletions, frame shifts, and splicing alterations. These *WDR19* mutations resulted in a broad range of symptoms, including arRP, NHPH, Sensenbrenner syndrome, Jeune syndrome, and Caroli syndrome, which involved multiple cilia-related organs and tissues, including the retina, kidneys, liver, and bone (Table 2). Hence, the phenotypes associated with *WDR19* mutations are diverse with a broad phenotypic and severity spectrum in various ciliopathies. However, *WDR19* mutation had not been previously examined in the context of male infertility.

In this study, we identified a novel homozygous mutation of *WDR19* in an individual resulting from a consanguineous

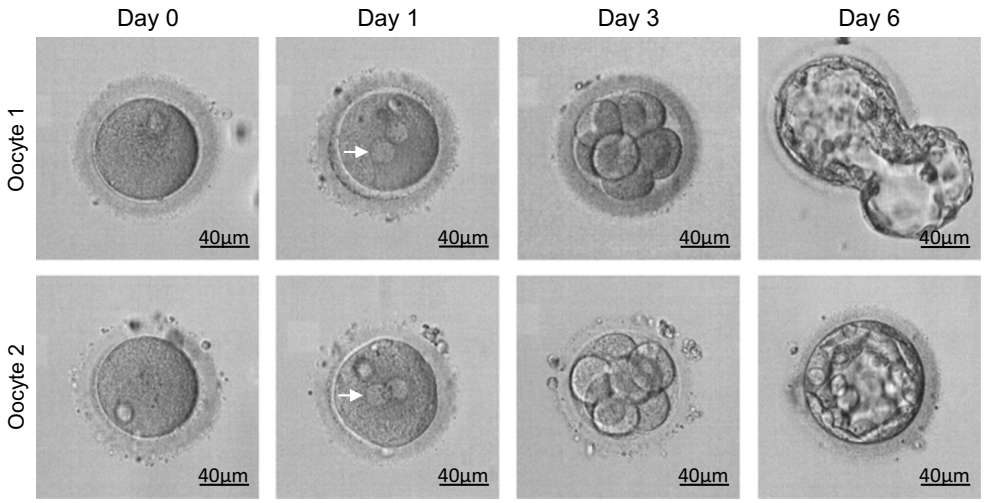

Fig. 3 ICSI outcome of *WDR19*-mutated patient. Eleven metaphase II oocytes were retrieved from the wife of the *WDR19*-mutated patient and 8 of them were fertilized with the WDR19-deficient sperm by ICSI. Fertilized oocytes were cultured 6 days after ICSI. Fortunately, they obtained 2 good quality blastocysts (5BB, 3BB), which were transferred in a frozen cycle and resulted in successful pregnancy. White arrows indicate the pronuclei. Scale bar: 40 μm

Table 2 Summary of the patients carrying *WDR19* mutations in previous studies

Patient	Ethnicity	Gender	Zygosity	Mutation 1	Protein/RNA change 1	Mutation 2	Protein/RNA change 2	Diagnostics	PMID	Consanguinity
1	Norwegian	Female	CHet	c.2129T>C	p.Leu710Ser	c.3307C>T	p.Arg1103*	Sensenbrenner	22,019,273	No
2	Norwegian	Male	CHet	c.2129T>C	p.Leu710Ser	c.3307C>T	p.Arg1103*	Sensenbrenner	22,019,273	No
3	Dutch	Female	Hom	c.20T>C	p.Leu7Pro	c.20T>C	p.Leu7Pro	Jeune	22,019,273	No
4	Moroccan	Male	CHet	c.1034T>G	p.Val345Gly	c.3068dupA	p.Tyr1023*	NPHP	22,019,273	No
5, 6, 7	Moroccan	Female	CHet	c.1034T>G	p.Val345Gly	c.3068dupA	p.Tyr1023*	NPHP	22,019,273	No
8	Korean	Male	CHet	c.3533G>A	p.Arg1178Gln	c.3703G>A	p.Glu1235Lys	NPHP and Caroli	25,726,036	No
9, 10	Korean	Female	CHet	c.3533G>A	p.Arg1178Gln	c.3703G>A	p.Glu1235Lys	NPHP and Caroli	25,726,036	No
11	Korean	Male	CHet	c.3533G>A	p.Arg1178Gln	c.1483G>T	p.Gly495Cys	NPHP and Caroli	25,726,036	No
12	Korean	Male	CHet	c.3533G>A	p.Arg1178Gln	c.1853 T>C	p.Leu618Pro	NPHP and Caroli	25,726,036	No
13	Korean	Female	Hom	c.3533G>A	p.Arg1178Gln	c.3533G>A	p.Arg1178Gln	NPHP and Caroli	25,726,036	No
14	Philippine	Female	Hom	c.1483G>C	p.Gly495Arg	c.1483G>C	p.Gly495Arg	Multiple malformations	24,504,730	No
15	French-Canadian	Male	Hom	c.2129T>C	p.Leu710Ser	c.2129T>C	p.Leu710Ser	RP	23,683,095	Yes
16	French-Canadian	Female	Hom	c.2129T>C	p.Leu710Ser	c.2129T>C	p.Leu710Ser	RP	23,683,095	No
17	Canadian	NA	Het	c.641dupT	p.Leu214PhefsX5	c.1477G>C	p.Asp493His	NPHP and RP	23,683,095	No
18	Canadian	NA	Het	c.203T>A	p.Val68Asp	c.407-2A>G	Splice site	NPHP and RP	23,683,095	No
19	Canadian	NA	Het	c.88G>C	p.Ala30Pro	WT	WT	NPHP and RP	23,683,095	No
20	Canadian	NA	Het	c.326G>A	p.Gly109Glu	WT	WT	NPHP and RP	23,683,095	No
21	Canadian	NA	Het	c.781dupA	p.Thr261AsnfsX13	WT	WT	NPHP and RP	23,683,095	No
22	Japanese	Female	CHet	c.953delA	p.Asn319Ilefs*16	c.3533G>A	p.Arg1178Gln	NPHP	28,621,010	No
23	Japanese	Female	CHet	c.2645+1G>T	Splice site	c.3533G>A	p.Arg1179Gln	Polycystic kidney disease	28,621,010	No

CHet, compound heterozygous; *Het*, heterozygous; *Hom*, homozygous. *WT*, wide type; *NPHP*, nephronophthisis; *Caroli*, Caroli syndrome; *Sensenbrenner*, Sensenbrenner syndrome, *Jeune*, Jeune syndrome; *RP*, retinitis pigment; *NA*, not available

union. This patient only presented with sterility caused by asthenoteratospermia, without any of the aforementioned ciliopathy symptoms. Analysis of semen revealed a complete loss of flagellar motility, while ultrastructural images of sperm flagella showed complete damage in the flagella. Given that the patient did not present with PCD-related symptoms and that biopsies are an invasive procedure, we were unable to obtain cilia from other tissues to examine its morphology. Nevertheless, systemic examination revealed no obvious abnormalities in the bones, teeth, liver, kidneys, fundus, and respiratory tract. Therefore, we speculated that at least partial ciliary function was retained in the patient.

This unusual disease phenotype resulting from the observed homozygous *WDR19* mutation may be the result of numerous factors. Firstly, the type and location of the gene variant may influence factors of the disorders. Karel et al. reported that weak and strong alleles of *WDR19*/*IFT144* elicit distinct effects on axoneme structure [11]. In this study, the *WDR19* mutation occurred near the C-terminus and was identified as a missense mutation (potentially a hypomorphic mutation), and as such would have only minimal effects on protein structure and function. To our knowledge, this is the only *WDR19* mutation occurring in the DZR domain (consists of two zinc finger structures; Fig. 1), which is the last domain of WDR19. The clinical and ciliary phenotypes in this patient are less severe when compared with the phenotypes in patients with multiple anomaly syndrome. This difference corresponds to the identification of a milder genetic defect. Secondly, sperm flagella formation may not be entirely consistent with cilia formation, which has been observed in mouse models. Mice with knock-down of various *Bbs* genes fail to form sperm flagella yet effectively form primary cilia in other organs [12–14]. Thirdly, the high propensity for genetic modification, genetic loading, modifier effects, and oligogenic inheritance in ciliopathies, which all refer to the likelihood that mutations in more than one gene affect phenotype, have also been proposed as explanations for the clinical variability within ciliopathies and within families suffering from these disorders [15–17].

IFT140 and IFT88 are components of IFT-A complex and IFT-B complexes, respectively. In silico software String analysis shows that IFT-140 and IFT88 have direct interactions with WDR19. In order to investigate the effect of WDR19 deficiency on the IFT-A complex and IFT-B complexes, we carried out immunofluorescence staining of IFT140 and IFT88 on the sperm from the *WDR19*-mutated patient. The results showed that the expression level or location of IFT140 and IFT88 differed significantly from the controls, and the expression level or location of IFT140 in the sperm from the *WDR19*-mutated patient and the control men was more significant. This result is consistent with the prediction of the tighter interaction between IFT140 and WDR19. Hence, the *WDR19* mutation may lead to the abnormal expression of other IFT partials, thereby causing eventual damage and disorganization of microtubule structures in flagella. Furthermore, sperm-associated antigen 6 (SPAG6) is reported to be important for structural integrity of the central apparatus in the sperm tail and for flagellar motility. It is showed that SPAG6 was approximately absent in the sperm of *WDR19*-mutated patient. This result was consistent with the absence of central pair of microtubules observed by TEM.

Assisted reproduction techniques (ART), such as IVF and ICSI, have become important tools for treating infertile couples [18]. To date, no reported empirical medicinal treatment could improve the semen parameters for those patients affected by MMAF-associated asthenoteratospermia; therefore, ICSI could be the only choice for those couples [19]. However, previous studies have shown that MMAF patients with different mutations have different prognosis after ICSI. For example, the patients with *DNAH1*- and *SUN5*-associated MMAF have good clinical outcomes following ICSI [20, 21]. In contrast, a *CEP135*-associated MMAF subject had a failed pregnancy [22]. Therefore, comparative studies on ICSI outcomes between different MMAF-associated genes would be informative to clinicians before ART treatment recommendation. Fortunately, in this study, subject with *WDR19* mutation had a successful clinical pregnancy following ICSI with his own sperm. Our findings indicate that ICSI can be recommended for WDR19-associated asthenoteratospermia, which may provide guidance for future treatment of such patients.

Conclusion

In summary, our findings demonstrate that *WDR19* homozygous missense mutation can induce asthenoteratospermia characterized by reduced sperm motility and multiple sperm structural malformations. Fortunately, a good pregnancy outcome could be acquired through ICSI in the *WDR19*-mutated man. Since the incidence of *WDR19* deleterious mutation is very low in the general population, we have not identified additional patients carrying *WDR19* mutations, which is a primary limitation of this study. However, the detailed molecular contributions of WDR19 to sperm flagellar formation and intraflagellar transport must be further investigated in future studies.

Acknowledgments We would like to thank the families who participated in and supported this research.

Authors' Contributors YC, FZ, XH, and XN designed the study. XN, JW, YZ, HW, YG, QT, BC, QL, BS, ZW, and ZZ provided patients' data and performed clinical assessments. XN, ML, JW, ST, CL, HC, YG, YC, and QT conducted the experiments. XN, XH, ML, ST, and JW analyzed the data. XN and XH wrote the manuscript. YC, FZ, and XH were

responsible for the study supervision. All authors read and approved the final manuscript.

Funding This study was supported by the Special Foundation for Development of Science and Technology of Anhui Province (grant number 2017070802D150), the Natural Science Foundation of Anhui Province (grant numbers 1708085QC59 and 1908085QH313), the Non-profit Central Research Institute Fund of Chinese Academy of Medical Sciences (2019PT310002), and the University Synergy Innovation Program of Anhui Province (GXXT-2019-044).

Compliance with ethical standards

Competing interests The authors declare that they have no competing interests.

Patient consent All patients provided their signed informed consent for this study.

Provenance and peer review Not commissioned; externally peer reviewed.

Data sharing statement Additional unpublished data.

Ethics approval The Ethical Committee of Anhui Medical University (PJ2017-11-10).

References

1. Baccetti B, Collodel G, Estenoz M, Manca D, Moretti E, Piomboni P. Gene deletions in an infertile man with sperm fibrous sheath dysplasia. Hum Reprod. 2005;20(10):2790–4.
2. Pedersen LB, Rosenbaum JL. Intraflagellar transport (IFT) role in ciliary assembly, resorption and signalling. Curr Top Dev Biol. 2008;85:23–61.
3. Buisson J, Chenouard N, Lagache T, Blisnick T, Olivo-Marin JC, Bastin P. Intraflagellar transport proteins cycle between the flagellum and its base. J Cell Sci. 2013;126(Pt 1):327–38.
4. Efimenko E, Blacque OE, Ou G, Haycraft CJ, Yoder BK, Scholey JM, et al. Caenorhabditis elegans DYF-2, an orthologue of human WDR19, is a component of the intraflagellar transport machinery in sensory cilia. Mol Biol Cell. 2006;17(11):4801–11.
5. Cooper TG, Noonan E, von Eckardstein S, Auger J, Baker HW, Behre HM, et al. World Health Organization reference values for human semen characteristics. Hum Reprod Update. 2010;16(3):231–45.
6. He X, Li W, Wu H, Lv M, Liu W, Liu C, et al. Novel homozygous CFAP69 mutations in humans and mice cause severe asthenoteratospermia with multiple morphological abnormalities of the sperm flagella. J Med Genet. 2019;56(2):96–103.
7. Liu W, He X, Yang S, Zouari R, Wang J, Wu H, et al. Bi-allelic mutations in TTC21A induce asthenoteratospermia in humans and mice. Am J Hum Genet. 2019;104(4):738–48.
8. Auger J, Jouannet P, Eustache F. Another look at human sperm morphology. Hum Reprod. 2016;31(1):10–23.
9. Liu H, Li W, Zhang Y, Zhang Z, Shang X, Zhang L, et al. IFT25, an intraflagellar transporter protein dispensable for ciliogenesis in somatic cells, is essential for sperm flagella formation. Biol Reprod. 2017;96(5):993–1006.
10. Zhang Y, Liu H, Li W, Zhang Z, Shang X, Zhang D, et al. Intraflagellar transporter protein (IFT27), an IFT25 binding partner, is essential for male fertility and spermiogenesis in mice. Dev Biol. 2017;432(1):125–39.
11. Liem KF Jr, Ashe A, He M, Satir P, Moran J, Beier D, et al. The IFT-A complex regulates Shh signaling through cilia structure and membrane protein trafficking. J Cell Biol. 2012;197(6):789–800.
12. Fath MA, Mullins RF, Searby C, Nishimura DY, Wei J, Rahmouni K, et al. Mkks-null mice have a phenotype resembling Bardet-Biedl syndrome. Hum Mol Genet. 2005;14(9):1109–18.
13. Mykytyn K, Mullins RF, Andrews M, Chiang AP, Swiderski RE, Yang B, et al. Bardet-Biedl syndrome type 4 (BBS4)-null mice implicate Bbs4 in flagella formation but not global cilia assembly. Proc Natl Acad Sci U S A. 2004;101(23):8664–9.
14. Nishimura DY, Fath M, Mullins RF, Searby C, Andrews M, Davis R, et al. Bbs2-null mice have neurosensory deficits, a defect in social dominance, and retinopathy associated with mislocalization of rhodopsin. Proc Natl Acad Sci U S A. 2004;101(47):16588–93.
15. Thiel C, Kessler K, Giessl A, Dimmler A, Shalev SA, von der Haar S, et al. NEK1 mutations cause short-rib polydactyly syndrome type Majewski. Am J Hum Genet. 2011;88(1):106–14.
16. Badano JL, Leitch CC, Ansley SJ, May-Simera H, Lawson S, Lewis RA, et al. Dissection of epistasis in oligogenic Bardet-Biedl syndrome. Nature. 2006;439(7074):326–30.
17. Hoefele J, Wolf MT, O'Toole JF, Otto EA, Schultheiss U, Deschenes G, et al. Evidence of oligogenic inheritance in nephronophthisis. J Am Soc Nephrol. 2007;18(10):2789–95.
18. Palermo G, Joris H, Devroey P, Van Steirteghem AC. Pregnancies after intracytoplasmic injection of single spermatozoon into an oocyte. Lancet. 1992;340(8810):17–8.
19. Chemes HE, Alvarez SC. Tales of the tail and sperm head aches: changing concepts on the prognostic significance of sperm pathologies affecting the head, neck and tail. Asian J Androl. 2012;14(1):14–23.
20. Wambergue C, Zouari R, Fourati Ben Mustapha S, Martinez G, Devillard F, Hennebicq S, et al. Patients with multiple morphological abnormalities of the sperm flagella due to DNAH1 mutations have a good prognosis following intracytoplasmic sperm injection. Hum Reprod 2016;31(6):1164–1172.
21. Zhu F, Wang F, Yang X, Zhang J, Wu H, Zhang Z, et al. Biallelic SUN5 mutations cause autosomal-recessive acephalic spermatozoa syndrome. Am J Hum Genet. 2016;99(4):942–9.
22. Sha YW, Xu X, Mei LB, Li P, Su ZY, He XQ, et al. A homozygous CEP135 mutation is associated with multiple morphological abnormalities of the sperm flagella (MMAF). Gene. 2017;633:48–53.